IEEE Access
Multidisciplinary | Rapid Review | Open Access Journal

Received May 21, 2021, accepted June 17, 2021, date of publication June 28, 2021, date of current version July 5, 2021.

Digital Object Identifier 10.1109/ACCESS.2021.3092887

Winding Resistance Measurement in Power Inductors - Understanding the Impact of the Winding Mutual Resistance

ERNESTO L. BARRIOS, (Member, IEEE), DAVID ELIZONDO, (Student Member, IEEE), ALFREDO URSÚA, (Senior Member, IEEE), AND PABLO SANCHIS, (Senior Member, IEEE)
Department of Electrical, Electronic and Communications Engineering, Public University of Navarre, 31006 Pamplona, Navarra, Spain

Corresponding author: Ernesto L. Barrios (ernesto.barrios@unavarra.es)

This work was supported in part by the Spanish State Research Agency (AEI) and the FEDER-UE under Grant PID2019-110956RB-I00/AEI/10.13039/501100011033, and in part by the Ingeteam Power Technology.

ABSTRACT Inductors are cornerstone components in power electronics converters. Since winding loss is the dominant loss mechanism in these components, its accurate measurement is fundamental for the validation of the inductor's operation and design. The techniques for the winding resistance R_w measurement in power inductors can be classified into two groups, indirect and direct. Both techniques use coupled inductors to separate winding and core power losses. If coupled inductors with non-zero winding mutual resistances $R_{w,m}$ are used, invalid results are obtained with these techniques. Understanding the meaning of $R_{w,m}$ in coupled inductors is complex. In this paper, the impact of $R_{w,m}$ on the inductor R_w measurement techniques is demonstrated and practical guidelines for the design of the zero $R_{w,m}$ coupled inductors are given. Particularly, the location of the auxiliary winding for the direct technique is investigated. In order to compare the R_w measurement techniques and to validate the coupled inductor's $R_{w,m}$ impact, two different inductors are built and tested. The results are compared with the values for R_w calculated by FEA simulation. It is found that only the direct technique with an auxiliary winding carefully designed and located following the guidelines given in this paper makes the accurate measurement of R_w in power inductors possible.

INDEX TERMS Inductor, coupled inductor, winding resistance, mutual resistance, loss measurement, measurement technique, measurement uncertainty.

I. INTRODUCTION

Inductors are key components in the operating principle of most industrial power electronics converters such as EV chargers [1], [2], PFC rectifiers [3], traditional single-phase SMPS [4], and low-power and multi-megawatt inverters for distributed and centralized renewable energy generation systems [5]–[7]. Inductors strongly influence the volume, weight, cost and efficiency of these converters [8]–[10]. In consequence, inductor design and validation are critical steps in the converter design process and operation. Power loss during the inductor operation leads to a temperature increase that delimits its size and its stored energy density capability [11], [12] and in consequence its cost [8]. In addition to this, inductor power loss negatively impacts the converter efficiency increasing its life cycle cost [9].

Power loss in an inductor is divided into winding and core losses. Inductor design can be saturation-constrained, typically in dc-dc converters and grid frequency applications with large dc or low frequency current components, or thermally-constrained, typically in applications with large or only high frequency components [10]. In the first case, winding loss is predominant over core loss [11], while in the second case winding loss and core loss are similar [10]. Thus, winding loss estimation and validation are fundamental in the design and correct operation of any kind of inductor.

There are a large number of models to estimate inductor winding resistance, R_w, depending on the winding-core-gap geometrical arrangement. Some examples can be found in [10], [13]–[17]. However, it is even more important to

The associate editor coordinating the review of this manuscript and approving it for publication was Chi-Seng Lam.

have R_w measurement techniques available that enable experimental validation of these models. These techniques are also useful to test a given inductor and to validate its correct design and assembly. Another important advantage of knowing R_w is that it enables the extraction of the inductor core loss under real operation from a total loss measurement [18].

The main challenge when measuring R_w is to successfully separate the inductor winding loss from its core loss. The R_w measurement techniques can be classified into two groups, the indirect and the direct techniques. In the indirect technique, R_w is obtained as a combination of different measured resistances, while in the direct technique, R_w is directly measured. The indirect technique follows 3 steps [19], [20]:

1) *Step 1*: Measure the total inductor resistance under a small-signal sinusoidal excitation.
2) *Step 2*: Measure the same core resistance existent in the previous test by means of an auxiliary coupled inductor.
3) *Step 3*: Subtract the core resistance from the total resistance.

If the three steps are properly executed, which is not a straightforward task, R_w is obtained. However, two measurements of the resistive part of impedances with phases very close to 90° are combined often leading to a high measurement uncertainty. The uncertainty is further deteriorated in this technique if the core loss measured in *step 2* is a relevant percentage (more than 10%) of the total resistance measured in *step 1* [19]. Thus, for certain types of inductors commonly used in power electronics, it is not unusual to obtain uncertainties higher than 100% at medium frequencies even when dedicated high-cost impedance analyzers are used [21]. This means that the indirect technique is not always valid for the R_w measurement.

As an alternative, the direct technique uses an auxiliary winding wound on the original inductor to form a coupled inductor and to enable the separation of winding and core power losses thanks to a specific connection. The idea behind this technique is to be able to directly measure the leakage impedance of the *transformer* formed thanks to the auxiliary winding [21]. As a result, only one impedance needs to be measured with a phase far below 90° leading to low measurement uncertainty independently of the relevance of the core loss in the total inductor power loss. This is an important advantage over the indirect technique.

Both measurement techniques use coupled inductors to separate winding and core power losses. In coupled inductors, the windings are linked not only by a mutual inductance and a core mutual resistance but also by means of a winding mutual resistance $R_{w,m}$ [20], [22], and [23]. This mutual resistance models the fact that when two *ac* currents are present in two coupled windings, the winding loss is not only the sum of each of the winding losses calculated individually, but that an extra power loss due to the cross terms of the currents of the two windings also exists. As will be shown in this paper, $R_{w,m}$ *appears* in the measurements even when a current is flowing only through one winding. This $R_{w,m}$ causes an important error in the measured R_w. This fact has already been analyzed for the indirect technique in [20] concluding that a zero $R_{w,m}$ auxiliary coupled inductor must be used in *step 2*. However, this fact has not been analyzed or even reported for the direct technique. As will be demonstrated in this paper, in order to keep the advantages of the direct technique, an specific auxiliary winding with zero $R_{w,m}$ must be used. It is key then to properly understand the physical phenomenon represented by the winding mutual resistance. This way, it will be possible to build coupled inductors with zero $R_{w,m}$ that can assure a correct R_w measurement with both techniques.

This paper is organized as follows. In Section II, the electrical equivalent circuits for inductors and coupled inductors are explained in depth with a special focus on the modelling and understanding of the winding mutual resistance. By the end of the section, a specific coupled inductor equivalent circuit is proposed to facilitate the understanding and discussion of the different R_w measurement techniques. A review of the existing R_w measurement techniques, indirect and direct, is presented in Section III. In Section IV, the impact of the mutual winding resistance on the R_w measurement techniques is first studied. Then the conditions for zero $R_{w,m}$ coupled inductors that enable proper R_w measurement are investigated. Finally, the correct practical design and location for the auxiliary winding in the direct technique is presented. Section V carries out an experimental comparison of the two R_w measurement techniques and also the experimental validation of the auxiliary winding location for the direct technique. The different techniques are implemented and the measured R_w values are compared to the results obtained by means of FEA simulation. Two different types of inductors widely found in power electronics applications are tested showing the benefits of the direct R_w measurement technique but only if the auxiliary winding is designed and located following the indications given in this paper. Finally, conclusions are drawn in Section VI.

II. ELECTRICAL MODELLING OF INDUCTIVE DEVICES

A. INDUCTOR ELECTRICAL EQUIVALENT CIRCUIT

A physical representation of an inductor is shown in Fig. 1(a). The inductor consists in an electric conductor wound N times over a magnetic core with an effective relative permeability of u_{eff}. The relationship between the inductor voltage $\overrightarrow{V_L}$ and current $\overrightarrow{I_L}$ can be modelled as the inductor impedance $\overrightarrow{Z_L}$. An electrical equivalent circuit for inductors for sinusoidal

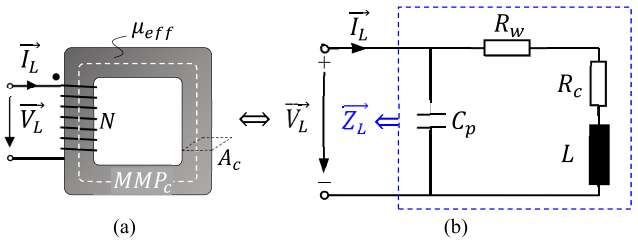

FIGURE 1. (a) Physical representation of an inductor. (b) Inductor electrical equivalent circuit.

excitation is shown in Fig. 1(b). In this circuit, the physical phenomena involved in the inductor operation are modelled by means of the self-inductance L, the winding and core series resistances, R_w and R_c respectively, and the parallel parasitic capacitance C_p.

The self-inductance relates the device's total magnetic flux to the current that generates it and can be calculated as:

$$L = L_c + L_{air} + L_w, \tag{1}$$

where each term represents the flux in the materials that form the inductor: in the core, L_c, in the air, L_{air}, and in the winding, L_w. In addition to the magnetic flux that circulates only through the air and through the winding, the last two terms also model the flux that flows partially through the core and that closes through the air or the winding. If only the dominant term in cored inductors is considered, by solving the magnetic circuit, the self-inductance can be expressed as a function of the device geometry and properties as follows:

$$L \approx L_c = \frac{N^2}{\mathcal{R}_c} = N^2 \frac{\mu_0 \mu_{eff} A_c}{MMP_c}, \tag{2}$$

where $\mathcal{R}_c$ is the core reluctance, A_c is the core section, MMP_c is the core mean magnetic path and μ_0 is the magnetic constant. The effective relative permeability used in inductors in power electronics applications is typically low (<150) in order to both avoid saturation and increase the stored energy density [11]. This can be made by using magnetic cores with an homogeneously distributed air gap such as powder cores, commonly toroidal cores [13], [24]–[26], or by including one or more lumped air gaps in high relative permeability cores such as amorphous, ferrites and nanocrystalline cores [12], [24], and [27].

The winding resistance R_w models the power loss P_w in the winding due to a *rms* current I_{rms} as:

$$R_w = \frac{P_w}{I_{rms}^2} = F_r \cdot R_{dc}, \tag{3}$$

where R_{dc} is the *dc* winding resistance (current density is homogeneously distributed in the wire section) and F_r is the resistance factor that models the winding loss increase with frequency when the inductor is excited by an *ac* current. When operating with *ac* current, the flux variation throughout the copper section induces eddy currents. As a consequence, the current density distribution in the winding volume $\boldsymbol{J}$ is non-homogeneous. The current density $\boldsymbol{J}$ can be expressed for sinusoidal waveforms in a generic way as:

$$\boldsymbol{J}(x, y, z, t) = J_p(x, y, z) \cos(\omega t + \varphi), \tag{4}$$

and can also be expressed as a spatial phasor $\vec{J}$ of magnitude J_p and phase φ. The non-homogeneous current density distribution leads to an effective increase in the winding loss. It is then convenient to keep in mind that the winding loss can be calculated as a function of the current density $\boldsymbol{J}$ as follows [28]:

$$\boldsymbol{J} \text{ sinusoidal with } t$$
$$\downarrow$$
$$P_w = \frac{1}{\sigma T} \int_{V_w} \int_0^T |\boldsymbol{J}|^2 \, dt \, dV_w = \frac{1}{2\sigma} \int_{V_w} \vec{J} \cdot \vec{J}^* dV_w$$
$$= \frac{1}{2\sigma} \int_{V_w} J_p^2 dV_w \tag{5}$$

where σ is the conductor conductivity considered homogeneous in the winding volume V_w, T is the period of the current waveform and * indicates the phasor conjugate. $\boldsymbol{J}$ depends on the geometry and properties of winding and core. For this reason, there is not a generic expression for the calculation of R_w in inductors. The calculation of R_w remains a topic of great interest. Some examples for different winding-core-gap arrangements can be found in [10], [13]–[17].

The core resistance R_c models the power loss in the magnetic core P_c due to a variable magnetization as follows:

$$R_c = \frac{P_c}{I_{rms}^2}. \tag{6}$$

Core loss can be empirically modelled with reasonable accuracy for a sinusoidal magnetization by means of the Steinmetz equation [29]:

$$P_c = C_m \cdot f^{\alpha} \cdot \int_{V_c} \boldsymbol{B}^{\beta} dV_c, \tag{7}$$

where C_m, α and β are empirical magnetic material loss coefficients, V_c is the core volume and $\boldsymbol{B}$ is the peak magnetic induction vector. Approximating $\boldsymbol{B}$ as homogeneous in the core volume and expressing it as a function of the inductor *rms* current that generates it, R_c can be expressed as:

$$R_c = 2^{\frac{\beta}{2}} \cdot V_c \cdot C_m \cdot f^{\alpha} \cdot \left(N \frac{\mu_0 \mu_{eff}}{MMP_c} \right)^{\beta} \cdot I_{rms}^{\beta - 2}. \tag{8}$$

This equation is equivalent to the one presented in [19] and is suitable when the core loss is modelled by means of a series resistance. R_c has been represented in series in the inductor circuit here because it enables the direct calculation of the core loss for a given current. Both representations, series and parallel, are valid and can be found indistinctly in the literature [19], [20], [30], and [31]. As established in (8), the inductor R_c value depends on the inductor current (*i.e.* the core magnetization) and the frequency. The core resistance also depends on the dc magnetization of the magnetic core. This fact can be included in (8) by making the coefficients C_m and β dependent on the dc bias magnetization [32].

The parasitic capacitance C_p models the electrical coupling between conductive objects in the winding. This lumped capacitance can satisfactorily model the effects of distributed parasitic capacitances, mainly turn-to-turn and layer-to-layer,

at low and medium frequencies [33]. The interaction of C_p with L causes the inductor self-resonance at frequency f_r:

$$f_r = \frac{1}{2\pi\sqrt{L \cdot C_p}}. \tag{9}$$

The impact of the self-resonance on the inductor operation cannot be neglected if the inductor operates with current components at frequencies in the vicinity of f_r. The calculation of C_p is not straightforward and is strongly dependent on the winding and core geometries [34].

B. COUPLED INDUCTOR ELECTRICAL EQUIVALENT CIRCUIT

In the different R_w measurement techniques, coupled inductors as the one shown in Fig. 2 are used. When two windings of N_1 and N_2 number of turns are wound on the same magnetic core, the device can be electrically modelled for sinusoidal excitation as shown in Fig. 3. In this model, the same elements as the ones in the inductor model in Fig. 1(b) are present for each of the windings. In Fig. 3, these elements are shown in black being L_1 and L_2 the self-inductances, $R_{c,1}$ and $R_{c,2}$ the core resistances and $R_{w,1}$ and $R_{w,2}$ the winding resistances, all of them for winding 1 and 2, respectively.

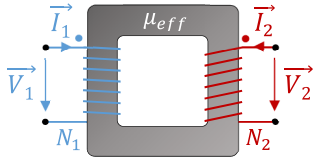

FIGURE 2. Physical representation of a two-winding coupled inductor used in R_W measurement techniques.

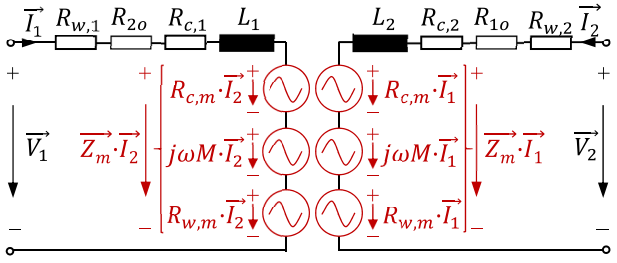

FIGURE 3. Two-winding coupled inductor electrical equivalent circuit for sinusoidal excitation.

However, as the windings are closely placed, resistances R_{1o} y R_{2o} need to be considered. These extra winding resistances are due to the induction *heating effect* [20]. When there is current only flowing through one winding and the other winding is in open circuit, proximity losses can be induced in the open-circuited winding leading to an increase in the resistance of the excited winding.

In addition, as the windings are wound on the same magnetic core, there exists a magnetic coupling between them. This coupling can be modelled as dependent voltage sources as shown in Fig. 3. The relationship between the voltage induced in one winding due to the current flowing through the other winding can be modelled as a mutual impedance $\vec{Z}_m$. Its imaginary part models the part of this voltage induced by the variation of the magnetic flux created by the current in the other winding and common to both windings. This inductive coupling is modelled by means of the mutual inductance M:

$$M = M_c + M_{air} + M_w, \tag{10}$$

where M_c, M_{air} and M_w are the mutual inductances due to the common fluxes through the core, the air and the winding volume, respectively. As the energy stored in a coupled inductor has to always be positive, the maximum value for M is delimited by $M^2 < L_1 L_2$ [35]. It is convenient then to define M by means of the magnetic coupling coefficient k_m as follows:

$$M = k_m\sqrt{L_1 L_2}, \tag{11}$$

with $0 < k_m < 1$. The more compact and geometrically similar the windings are, the higher their magnetic coupling is and the closer k_m is to 1.

If the power loss in the coupled inductor is to be modelled, the mutual impedance also has a real part that is formed of two components, the core mutual resistance $R_{c,m}$ and the winding mutual resistance $R_{w,m}$. These mutual resistances are a consequence of the non-linear dependence of winding loss on the current density and of core loss on the magnetic induction.

With respect to winding loss, it must be taken into account that the total current density $\boldsymbol{J}$ is now the vector sum of two current densities of different origin. Firstly, the current density distribution over the volume of both windings V_T due to the net current flowing through only winding 1 $\boldsymbol{J}_1$ and, secondly, the current density distribution over V_T due to the net current flowing through only winding 2 $\boldsymbol{J}_2$. Expressing $\boldsymbol{J}$ as the addition of $\boldsymbol{J}_1$ and $\boldsymbol{J}_2$ in (5), the total power loss in the windings for sinusoidal currents can be now calculated as:

$$P_w = \frac{1}{2\sigma}\int_{V_T}\left(\vec{J}_1+\vec{J}_2\right)\left(\vec{J}_1^{*}+\vec{J}_2^{*}\right)dV_T = \frac{1}{2\sigma}\int_{V_T}\left(J_{1,p}^2 + J_{2,p}^2 + \mathrm{Re}\left\{\vec{J}_1\cdot\vec{J}_2^{*}\right\} + \mathrm{Re}\left\{\vec{J}_2\cdot\vec{J}_1^{*}\right\}\right)dV_T. \tag{12}$$

In other words, the total winding loss is not only the sum of each of the winding losses calculated individually but also the power loss due to the cross terms. Solving the spatial phasors dot products and taking the real part, the cross terms in (12) are:

$$\mathrm{Re}\left\{\vec{J}_1\cdot\vec{J}_2^{*}\right\} = J_{1,p}J_{2,p}c_{12}\cos(\varphi_1-\varphi_2) \quad \text{and} \quad \mathrm{Re}\left\{\vec{J}_2\cdot\vec{J}_1^{*}\right\} = J_{2,p}J_{1,p}c_{21}\cos(\varphi_2-\varphi_1), \tag{13}$$

where c_{12} and c_{21} are coefficients that depend on the spatial situation of one vector with respect to the other but not on time (as windings are static in inductors) and φ_1 y φ_2 are the time phases for each current. Taking into account that

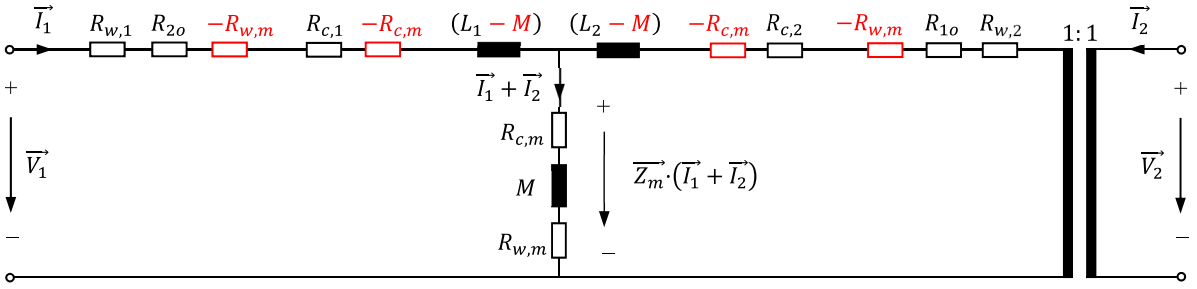

FIGURE 4. T model for a two-winding coupled inductor.

$\cos\varphi = \cos -\varphi$ and $c_{12} = c_{21}$ in each volume differential, the cross terms in (13) are equal and total winding loss is:

$$P_w = \frac{1}{2\sigma} \int_{V_T} \left(J_{1,p}^2 + J_{2,p}^2 + 2J_{1,p}J_{2,p}c_{12}\cos(\varphi_1 - \varphi_2) \right) dV_T. \tag{14}$$

Solving the integral throughout the volume of both windings, winding loss can be finally expressed as follows:

$$P_w = \left(R_{w,1} + R_{2o}\right) I_{rms,1}^2 + \left(R_{w,2} + R_{1o}\right) I_{rms,2}^2 + 2R_{w,m}\ \mathrm{Re}\left\{ \overrightarrow{I_{rms,1}} \cdot \overrightarrow{I_{rms,2}^*} \right\}. \tag{15}$$

Equation (15) is a well-known expression that can be found in [20], [22], and [23] among others. The extra coupling winding loss represented by the winding mutual resistance, its dependence on the phase shift between currents and its modelling still attract the researchers' attention today [22], [36], and [37].

Analogously, total core loss can be expressed as:

$$P_c \approx R_{c,1} I_{rms,1}^2 + R_{c,2} I_{rms,2}^2 + 2R_{c,m}\ \mathrm{Re}\left\{ \overrightarrow{I_{rms,1}} \cdot \overrightarrow{I_{rms,2}^*} \right\}. \tag{16}$$

As shown in (7), core loss is not proportional to the square of the magnetic induction. Thus, as in the case of the inductor, this difference is included and corrected in the different core resistances $R_{c,i}$ that therefore depend on the operating currents as expressed in (8).

From (14) and (16), it is clear why the mutual resistances need to be included in the equivalent circuit in Fig. 3. The total core and winding losses can never be negative and, as in the case of the mutual inductance, the maximum values for the mutual resistances are $R_{c,m}^2 < R_{c,1}R_{c,2}$ and $R_{w,m}^2 < (R_{w,1} + R_{2o})(R_{w,2} + R_{1o})$. It is interesting then to define the core loss coupling coefficient $k_{c,m}$ and the winding loss coupling coefficient $k_{w,m}$ as follows:

$$R_{c,m} = k_{c,m}\sqrt{R_{c,1}R_{c,2}}, \tag{17}$$

$$R_{w,m} = k_{w,m}\sqrt{\left(R_{w,1} + R_{2o}\right)\left(R_{w,2} + R_{1o}\right)}, \tag{18}$$

with $0 < k_{c,m} < 1$ and $0 < k_{w,m} < 1$. It should be clarified here that the magnetic coupling coefficient k_m and the core loss coupling coefficient $k_{c,m}$, despite being similar, are not the same. In order for two windings to have a k_m of 1, both windings must experience exactly the same magnetic flux. However, in order for two windings to have a $k_{c,m}$ of 1, it is enough that the magnetic flux in the core is common to both windings without being relevant whether the flux outside the core is common or not.

From a practical point of view, it is often convenient to avoid dependent voltage sources in order to make it easier to work with a circuit. For this purpose, a T model can be introduced as represented in Fig. 4, in which the two circuits are unified while the voltages and power balance are unchanged. The galvanic isolation between windings is represented by an ideal transformer with a unity turns ratio.

If both windings have the same number of turns (*i.e.* $N_1 = N_2$) and are wound in a way so that they generate a similar magnetic induction distribution in the core, the core resistance for winding 1 is very similar to the core resistance for winding 2, $R_{c,1} \approx R_{c,2}$. If, in addition, the two windings are wound in a way in which a high core loss coupling between windings is obtained ($k_{c,m} \approx 1$), from (17) the core mutual resistance is also very similar to the core resistance of each of the windings, $R_{c,m} \approx R_{c,1} \approx R_{c,2}$. Thus, in this case, the model from Fig. 4 can be simplified to the model in Fig. 5. This equivalent circuit will be used from now on in this paper since the coupled inductors used in the R_w measurement techniques always have the same number of turns for both windings and a high core loss coupling. In this model, the galvanic isolation is implicit and it is not represented as it is not relevant for the R_w measurement techniques.

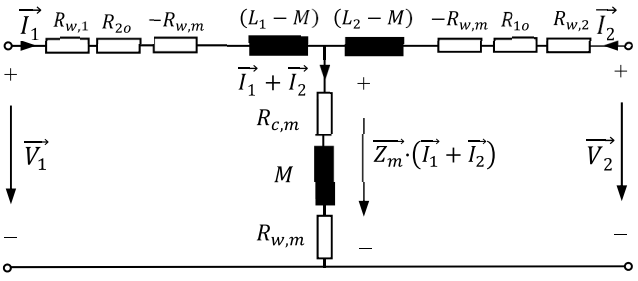

FIGURE 5. Simplified T model for a two-winding coupled inductor with the same number of turns and a high $k_{c,m}$. (galvanic isolation implicit).

As can be seen in Fig. 5, only a resistance is needed to model the power loss in the core. This core resistance is the core mutual resistance and only appears in the common circuit branch or in *parallel* as it is usually represented in transformer equivalent circuits. As a novelty, in the model presented in this paper the winding resistances are conveniently broken down according to their physical origin. These winding resistances are the addition of each winding self-resistance plus the high frequency proximity effects that exist due to the presence of other windings (induction heating effect and winding mutual resistance). It is also demonstrated here that the winding mutual resistance needs to be present in the parallel branch. Thus, the total resistance present in the parallel branch includes two different power loss mechanisms, one is the power loss in the core and the other one is a portion of the power loss in the windings.

III. R_W MEASUREMENT TECHNIQUES

A. INTRODUCTION

The main challenge when measuring R_w is to successfully separate the inductor winding loss from its core loss. The first approach that every engineer is tempted to follow consists in removing the core from the winding and directly measuring the resistance of the winding only. However, this is a mistake since, in the absence of the core, the flux lines in the winding volume are changed. As a consequence, it is very likely that $\boldsymbol{J}$ in (5) is strongly modified and that the measured R_w is not similar to the actual R_w of the original inductor [19], [21]. Another extended practice is to neglect the core loss under small signal excitation and, thus, to consider that the winding resistance equals the inductor total series resistance measured by means of an impedance analyzer. However, it has been demonstrated that this assumption can lead to important measurement errors even under small-signal excitation. This is due to the existence of a constant *remanent* core loss for very small core magnetization values (beyond 0.1 mT) [19].

Since the core cannot be removed and the core resistance is not negligible, R_w measurement techniques use a coupled inductor to separate winding and core losses. As mentioned in the introduction, these techniques can be classified into two groups, the indirect and the direct techniques. In the indirect technique, two measured resistances are combined to obtain the inductor's R_w, while in the direct technique, only one test is needed.

In the measurement techniques, impedances are measured by means of an impedance analyzer (Z Analyzer). The analyzer applies a small-signal sinusoidal excitation and performs a frequency sweep. No large signal test is needed, since, unlike the core resistance, the winding resistance does not depend on the magnetization level or the dc bias. Moreover, if the winding loss for a non-sinusoidal current is to be calculated, the power losses for each current harmonics can be calculated separately and by adding them together the total winding loss is obtained [38].

B. INDIRECT R_W MEASUREMENT

The indirect technique is the most common technique to measure inductor winding resistance and follows three steps [19], [20]:

- *Step 1*: Directly measure the inductor impedance under sinusoidal excitation for a given frequency range as shown in Fig. 6. The inductor self-resistance R_{wc}, which is the sum of core and winding resistances, is obtained as the real part of the measured inductor impedance $\overrightarrow{Z_{L,meas}}$. If the inductor self-resonance frequency in (8) is close to or even in the range in which R_w is to be measured, it is necessary to correct the effect of the parasitic capacitance C_p on the measured resistance as indicated in [19] or in [20].

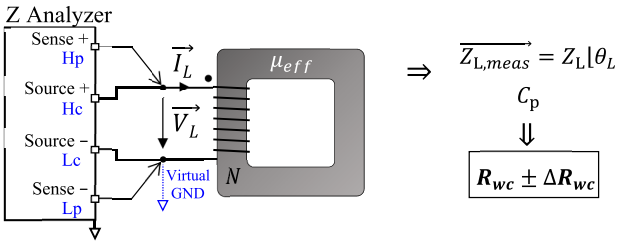

FIGURE 6. ***Step 1*** **in the indirect R_W measurement technique.**

- *Step 2*: Measure the core resistance existent in *step 1* in the same frequency range. For this purpose, the mutual impedance of a specific auxiliary coupled inductor is measured by exciting one winding and measuring the voltage induced in the other winding as shown in Fig. 7. The real part of the measured mutual impedance $\overrightarrow{Z_{m,meas}}$ is then extracted, $R_{c,aux} = \text{Re}\left\{\overrightarrow{Z_{m,meas}}\right\}$.

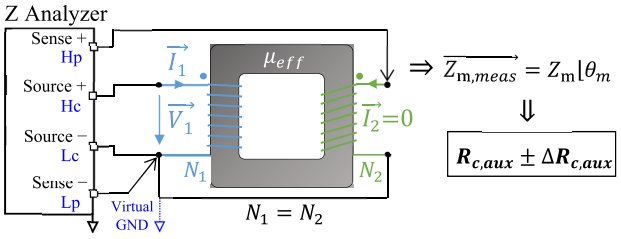

FIGURE 7. ***Step 2*** **in the indirect R_W measurement technique.**

Particularizing the coupled inductor model in Fig. 5 for the conditions of this test, the circuit in Fig. 8 is obtained. It can be seen that the measured resistance is actually the sum of core and winding mutual resistances, $R_{c,m}$ and $R_{w,m}$ respectively:

$$R_{c,aux} = \text{Re}\left\{\frac{\overrightarrow{V_{meas,2}}}{\overrightarrow{I_{meas,2}}}\right\} = R_{c,m} + R_{w,m}. \tag{19}$$

As the aim of this step is to obtain the original inductor core resistance R_c, it is necessary for the measured resistance $R_{c,aux}$ to equal R_c. For this purpose, the next characteristics are required for the auxiliary coupled inductor:

- To experience the same core loss as the original inductor, *i.e.* the coupled inductor $R_{c,m}$ must equal the original

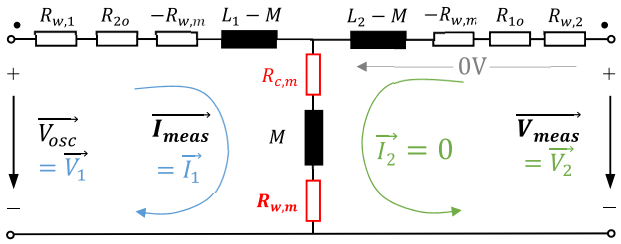

FIGURE 8. Equivalent circuit for *step 2* in the indirect technique.

inductor core resistance R_c (Fig. 1). For this purpose, the same core must be used with exactly the same core magnetization as the core resistance depends on the magnetization level.

- The minimum winding mutual resistance possible, $R_{w,m} \approx 0$.

- *Step 3*: Finally the core resistance measured in *step 2* $R_{c,aux}$ is subtracted from the total resistance measured in *step 1* R_{wc} and the measured winding resistance with the indirect technique $R_{w,i}$ is obtained:

$$R_{w,i} = R_{wc} - R_{c,aux}. \tag{20}$$

The main drawback of this method is that very high measurement uncertainty is obtained. Both measured resistances in *step 1* and *2* present high measurement uncertainties since the impedance phases to be measured θ are very close to 90° [21]. The relative uncertainty in the measurement of a resistance ΔR based on an impedance measurement, when only the influence of a deviation in the measured phase $\Delta\theta$ in rad (which is the main source of error) is considered, is [39]:

$$\frac{\Delta R}{R} = \tan\theta \cdot \Delta\theta \times 100\%. \tag{21}$$

Applying (21) for a power inductor with an 89.8° phase and considering a source of error of 4 ns of uncompensated total delay between voltage and current, the measurement uncertainty for the resistance (*e.g.* R_{wc} in *step 1*) is 10% at 20 kHz and beyond 100% at 200 kHz.

In addition, the subtraction performed in *step 3* magnifies the final measurement uncertainty. When subtracting two measurements their uncertainties are combined as follows (considering uncorrelated errors):

$$\Delta R_w = \sqrt{\Delta R_{wc}^2 + \Delta R_{c,aux}^2}. \tag{22}$$

As the result of a subtraction is always a lower value ($R_{w,meas} < R_{wc}$) and the uncertainty has been propagated ($\Delta R_w > \Delta R_{wc}$), the final measurement relative uncertainty increases:

$$\frac{\Delta R_w}{R_{w,meas}} \gg \frac{\Delta R_{wc}}{R_{wc}}. \tag{23}$$

This magnifying effect is more relevant the higher the percentage of the core loss is in the inductor total loss. Therefore, it can be very important in high-frequency magnetic materials with *high* core loss such as powder cores.

In order to reduce the measurement uncertainty in *step 2*, and thus the final measurement uncertainty, it is common to eliminate the air gap in the auxiliary coupled inductor used for measuring R_c in this step [40]. In this way, the quality factor Q is reduced leading to a lower impedance phase. This process is not straightforward and is explained in detail in [20]. This approach generally leads to very good results, however it cannot be always applied. When using powder cores, the air gap cannot be removed as it is homogeneously distributed within the core. In addition, when lumped gaps or multigaps are present in some magnetic materials the core loss is increased. Examples are given for nanocrystalline cores with a single gap in [27] and [41] and for ferrite cores with multiple gaps in [31]. In these cases, the gap cannot be removed without modifying the core resistance and then the measurement uncertainty in *step 2* cannot be reduced.

C. DIRECT R_W MEASUREMENT

To overcome the limitations of the indirect technique, the direct technique avoids the combination of several measurements with impedance phases close to 90° [21]. Only one test with the specific connection shown in Fig. 9 is needed to measure R_w. In this test, an auxiliary winding with the same number of turns as the original inductor winding is wound on the original inductor. The idea behind this technique is to directly measure the leakage impedance of the *transformer* formed thanks to the auxiliary winding.

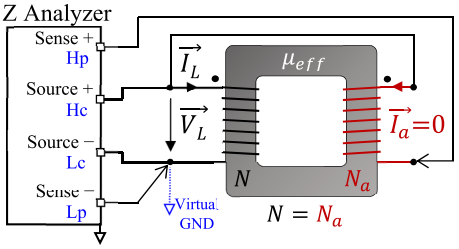

FIGURE 9. Direct R_W measurement technique.

In order to properly understand this technique, the coupled inductor model in Fig. 5 is particularized for the conditions of the test in Fig. 9 obtaining the circuit shown in Fig. 10. The series elements are drawn in the bottom part of the equivalent circuit for the sake of clarity since in the direct technique the corresponding terminals are short circuited. From Fig. 10, it can be seen that the impedance measured with the direct technique $\overrightarrow{Z_d}$ is as follows:

$$\overrightarrow{Z_d} = \frac{\overrightarrow{V_{meas}}}{\overrightarrow{I_{meas}}} = R_w + R_{ao} - R_{w,m} + j\omega\,(L - M)\,. \tag{24}$$

Indeed, thanks to the coupling obtained with the auxiliary winding, the direct technique enables:

– The separation of winding and core losses without the need of an auxiliary coupled inductor.
– A reduction in the measurement uncertainty since only one impedance measurement is necessary with a phase far

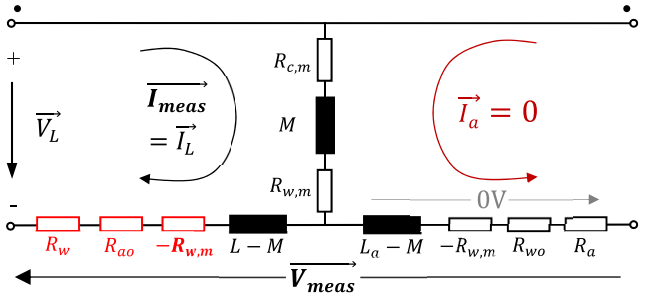

FIGURE 10. Equivalent circuit for the direct R_W measurement technique.

below 90°. The inductive character of the impedance is considerably reduced thanks to the effect of the coupling since $(L - M) \ll L$.

The measured winding resistance with the direct technique $R_{w,d}$ is the real part of the measured impedance Z_d:

$$R_{w,d} = \mathrm{Re}\left\{\frac{\overrightarrow{V_{meas}}}{\overrightarrow{I_{meas}}}\right\} = R_w + R_{ao} - R_{w,m}. \quad (25)$$

It can be seen that the measured resistance is actually the sum of the original inductor winding resistance R_w and the resistance due to the induction *heating effect* in the auxiliary winding R_{ao}, minus the winding mutual resistance between the original and the auxiliary windings $R_{w,m}$. Thus, and thanks to the model proposed in this paper, it can be easily understood that the direct technique does not successfully measure the inductor winding resistance unless the next requirements are fulfilled:

- The minimum induction *heating effect* resistance possible for the auxiliary winding, $R_{ao} \approx 0$.
- The minimum winding mutual resistance possible, $R_{w,m} \approx 0$.

IV. INFLUENCE OF $R_{W,M}$ IN THE R_W MEASUREMENT

A. THE IMPORTANCE OF $R_{W,M}$

In both, indirect and direct R_w measurement techniques, the winding mutual resistance $R_{w,m}$ plays an important role. In the indirect technique, the $R_{w,m}$ of the auxiliary coupled inductor is measured in *step 2*, while in the direct technique, the $R_{w,m}$ between the original winding and the auxiliary winding is directly included in the measurement. In both techniques it is necessary for these mutual resistances to be zero to successfully measure the inductor R_w. In the indirect technique, a non-zero $R_{w,m}$ in the auxiliary coupled inductor leads to an error in the measurement of the core loss and thus a deviation in the measured winding resistance $R_{w,i}$ obtained in *step 3*. In the direct technique, a non-zero $R_{w,m}$ directly leads to a deviation in the measured winding resistance $R_{w,d}$.

Practical guidelines to build an auxiliary inductor with minimal $R_{w,m}$ to be used in *step 2* of the indirect technique can be found in the literature [19], [20]. Techniques for measuring the core loss by means of coupled inductors as the one in [42] also address this issue. The guidelines for a minimum $R_{w,m}$ in a coupled inductor are: to use wires with the minimum diameter possible [19], [20], [42], to place the wires far away from each other [42] and even to use only one turn per winding [20]. However, no theoretical justification of these guidelines is given meaning that the understanding of the physical phenomenon represented by $R_{w,m}$ is limited.

In the direct technique, the existence of the winding mutual resistance has not been analyzed. As a consequence, there are no guidelines or indications on how to wind the auxiliary winding. Only a very thin wire is recommended in [21] in order to fit the auxiliary winding in the core window, but no more indications can be found. However, and as is going to be demonstrated in this paper, if the auxiliary winding is *randomly* wound, a non-zero $R_{w,m}$ will most likely be obtained. In that case, the direct winding technique leads to an unacceptable measurement deviation and its inherent advantages over the indirect technique are lost.

B. ZERO $R_{W,M}$ BETWEEN COUPLED WINDINGS, IS IT POSSIBLE?

A zero $R_{w,m}$ is key to the success of any of the two R_w measurement techniques. Only by properly understanding the loss mechanism represented by $R_{w,m}$, its value can be minimized. For this purpose, we can consider the total winding loss in a two winding device due to sinusoidal currents presented in (14). As it is of interest to know how the characteristics of each of the windings impact the $R_{w,m}$ value, it is convenient now to study the power loss in each of the windings separately. The total winding volume V_T is then split into the volume of winding 1 V_1 and the volume of winding 2 V_2. In the same way as in (14), the total current density is differentiated with respect to its origin. J_1 is the current density distribution (peak value) due to the net current flowing only through winding 1 and J_2 is the current density distribution (peak value) due to the net current flowing only through winding 2. The winding loss in winding 1 and in winding 2 are then respectively:

$$P_{w,1} = \frac{1}{2\sigma}\int_{V_1}\left(J_1^2 + J_2^2 + 2J_1J_2c_1\cos(\varphi_1 - \varphi_2)\right)dV_1, \quad (26)$$

$$P_{w,2} = \frac{1}{2\sigma}\int_{V_2}\left(J_2^2 + J_1^2 + 2J_1J_2c_2\cos(\varphi_1 - \varphi_2)\right)dV_2. \quad (27)$$

In both equations, the integral of the first term is the power loss in the winding due to its own current, modeled as the winding self-resistance, $R_{w,1}$ for winding 1 and $R_{w,2}$ for winding 2 in Fig. 5. The integral of the second term is the power loss in the winding due to a net current flowing through the other winding, modeled as R_{1o} for winding 1 and R_{2o} for winding 2 in Fig. 5. The integral of the third term is the power loss in the winding due to the coexistence of net currents flowing through both windings. Adding up the integrals of the third terms in (26) and (27), the total power loss due to the coexistence of net currents in both windings is obtained.

This power loss is modeled by means of the winding mutual resistance $R_{w,m}$ in Fig. 5.

In the tests performed in both R_w measurement techniques there is only a net current flowing through one winding. If we consider that winding 1 is excited while winding 2 is open circuited, J_2 does not exist and the power losses are in winding 1 due to its own current $R_{w,1}$ (first term in (26)) and in winding 2 due to the so called induction *heating effect* R_{1o} (second term in (27)). As there is no coexistence of net currents in both windings, there is no power loss due to the cross terms in (26) and (27) (third terms). This means that no net power is dissipated in the winding mutual resistances in Fig. 5 (the same current I_1 flows through $-R_{w,m}$ and $+R_{w,m}$). However, due to the way in which the voltage is measured, the mutual resistance $R_{w,m}$ does *appear* in the measurements and can result in incorrect R_w measurements. As established in Section III, to correctly measure R_w, in *step 2* of the indirect techniques (Fig. 8) $R_{w,m}$ needs to be zero. In the direct techniques (Fig. 10), not only $R_{w,m}$ but also R_{ao} needs to be zero (being the auxiliary winding the open circuited winding).

There are two ways to obtain a zero $R_{w,m}$ between two windings. One option is that the current densities due to the net currents of the different windings are orthogonal in space and, in consequence, its dot product is zero (meaning c_1 in (26) and c_2 in (27) are zero). This is very difficult to obtain in a practical way. The second and more practical option is that the current density in winding 2 induced by a net current flowing through winding 1 (J_1 in (27)) is zero and that the current density in winding 1 induced by a net current flowing through winding 2 is zero as well (J_2 in (26)). In other words, both windings must not modify each other's current densities which means that there is no proximity effect between them ($k_{w,m} = 0$ in (18)). As a consequence, the resistances due to the induction heating effect R_{1o} and R_{2o} will also be zero.

In *step 2* in the indirect technique, this is easy to obtain as the windings that form the auxiliary coupled inductor can be chosen freely. To minimize the proximity effect, it is enough to use windings with a diameter ϕ smaller than the minimum skin depth δ_{min} present in the test (corresponding to the highest frequency f_{max} to be tested):

$$\phi < \delta_{min} = \frac{1}{\sqrt{\pi \cdot f_{max} \cdot \mu_0 \cdot \sigma}}. \tag{28}$$

It is also advisable to place the windings far from each other and far from any possible air gap to minimize the magnetic flux variation through them. Thus, the guidelines that can be found in the literature are correct and are here justified.

In the direct technique, it is more difficult to achieve a zero $R_{w,m}$ since one of the windings is the original inductor winding (winding 1). This winding cannot be modified as its resistance R_w is to be measured. In a power inductor this winding has a considerable section and is affected by the fringing flux if lumped air gaps are present. To obtain a zero $R_{w,m}$ between original and auxiliary windings, two requirements are to be fulfilled. First, the diameter of the auxiliary winding must be small and fulfill (28). This way the current density in the auxiliary winding due to the net current flowing through the original winding (J_1 in (27)) is zero. Second, in order to minimize the current density in the original winding when a net current flows through the auxiliary winding (J_2 in (26)), the auxiliary winding must be wound in a very specific location. This location must be such that if an *ac* current circulates through the auxiliary winding it will not produce a varying magnetic field in the volume of the inductor original winding meaning that its current density will not be modified. This location is difficult to find but it does exist. As will be demonstrated in the next sections, the correct location depends on the inductor winding-core-gap geometrical arrangement and, thus, on the type of inductor.

C. AUXILIARY WINDING LOCATION FOR THE DIRECT R_W MEASUREMENT TECHNIQUE

In this paper, two types of inductors widely used in power electronics applications are considered. The first inductor type shown in Fig. 11(a) is a toroidal inductor with a homogenously distributed air gap and a low effective permeability μ_{eff}. The second inductor uses a magnetic material with high relative permeability μ_r that includes one or several lumped air gaps to reduce its effective permeability and prevent saturation. As shown in Fig. 11(b), a generic PM core with one gap in its central leg is considered here.

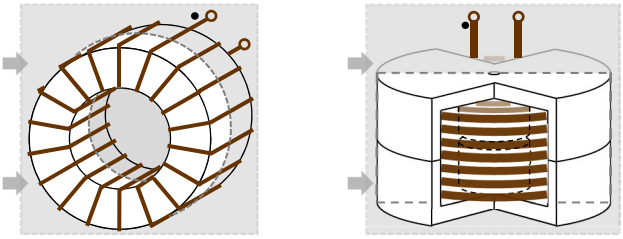

FIGURE 11. 3D representation of two common types of inductors for power electronics applications: (a) low μ toroidal inductor and (b) high μ PM gapped inductor.

For each of these types of inductors, two different locations for the auxiliary winding to be used in the direct technique are investigated. The first location has been carefully designed to achieve zero $R_{w,m}$ while the second location represents a case in which the auxiliary winding is wound without taking into account the winding mutual resistance. The different locations presented here are experimentally validated in Section V.

In Fig. 12, the cutting plane shown in Fig. 11(a) for the low μ toroidal inductor is schematically represented. Two locations are investigated for an auxiliary winding with a small diameter that fulfills (28). In the first one, shown in Fig. 12(a) and called *inside position*, the auxiliary winding is wound on the core and inside the power winding. This location leads to a zero $R_{w,m}$ and is then appropriate for the direct R_w

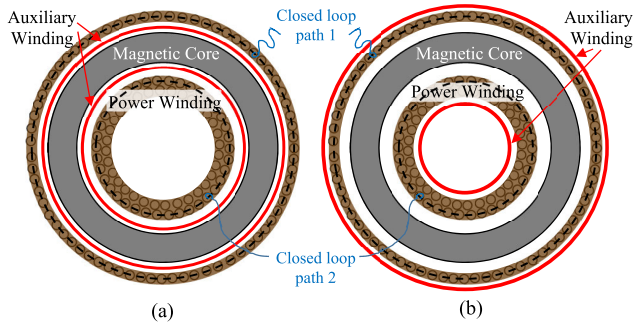

FIGURE 12. Two auxiliary winding locations for the inductor in Fig. 11(a): (a) *inside position* ($R_{w,m} \approx 0$) and (b) *outside position* (high $R_{w,m}$).

measurement technique. This fact can be understood by considering the magnetic field that would be created in the section of the original winding (power winding) when a net current circulates through the auxiliary winding. Ampere's law is applied to the two closed loop paths concentric to the windings shown in Fig. 12(a). In both cases, no magnetic field is obtained as the net current enclosed by the closed loops is zero. Thus, there is no eddy currents in the original winding as a consequence of a net current in the auxiliary winding.

In the second location called *outside position* and shown in Fig. 12(b), the auxiliary winding is directly wound over the power winding. Considering now the same two closed loop paths, it is easy to see that in this case a net current in the auxiliary winding produces a magnetic field in the original winding. If variable in time, the magnetic field induces a current density in the original winding given its big section. Thus, if the outside position is used for the auxiliary winding, the direct technique will lead to an incorrect R_w measurement due to the high $R_{w,m}$ between windings.

In Fig. 13, the cutting plane indicated in Fig. 11(b) for the high μ PM gapped inductor is schematically represented. Two locations are also investigated for the auxiliary winding. In the first one called *inside position* and shown in Fig. 13(a), the auxiliary winding is wound just over the air gap with the help of a non-magnetic non-conductive material piece placed in the gap. This location leads to a zero $R_{w,m}$ and is thus correct. This can be understood as follows, in this arrangement the magnetomotive force produced by a net current

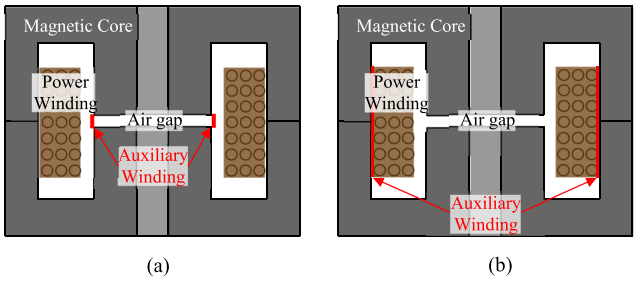

FIGURE 13. Two auxiliary winding locations for the inductor in Fig. 11(b): (a) *inside position* ($R_{w,m} \approx 0$) and (b) *outside position* (high $R_{w,m}$).

circulating through the auxiliary winding drops in the gap. This leads to a negligible magnetic field in the core window where the original winding is placed. As a consequence, eddy currents are not induced in the original winding due to a current in the auxiliary winding. One more regard is taken here due to the proximity of the auxiliary winding to the gap. When a current circulates through the original winding the auxiliary winding is exposed to an intense magnetic field due to the fringing flux. To avoid eddy currents in the auxiliary winding a further reduction of its diameter is necessary. We advise a diameter for the auxiliary smaller than half the minimum skin depth, $\phi_a < \delta_{min}/2$.

In the second location, shown in Fig. 13(b) and called *outside position*, the auxiliary winding is directly wound over the power winding. This location leads to a high $R_{w,m}$ and is thus incorrect. The reason is that a net current flowing through the auxiliary winding would produce a fringing flux that severely affects the original winding which in turn modifies its current density.

Thanks to the understanding of the physical phenomenon represented by $R_{w,m}$, it is been possible to analyze its impact on the R_w measurement techniques and, more importantly, to proposed practical guidelines for the correct design and location of the auxiliary winding to be used in the direct technique.

V. EXPERIMENTAL VALIDATION

A. INDUCTORS' CHARACTERISTICS AND TESTING METHODOLOGY

Two inductor prototypes that represent two types of inductors commonly used in power electronics applications are built and tested. Their winding resistances are calculated by simulation via software FEMM [43] and experimentally tested with the impedance analyzer E4990A 20Hz-120MHz from Keysight Technologies® [44]. A picture of each of the inductor prototypes is shown in Fig. 14 and their main characteristics are listed in Table 1.

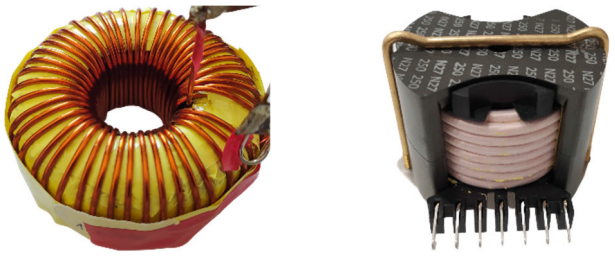

FIGURE 14. The two inductor prototypes: (a) low μ toroidal inductor and (b) high μ PM gapped inductor.

For each of the inductors, both indirect and direct R_w measurement techniques are applied. The obtained results are compared taking as a reference the R_w values calculated by simulation. The maximum desired measurement frequency

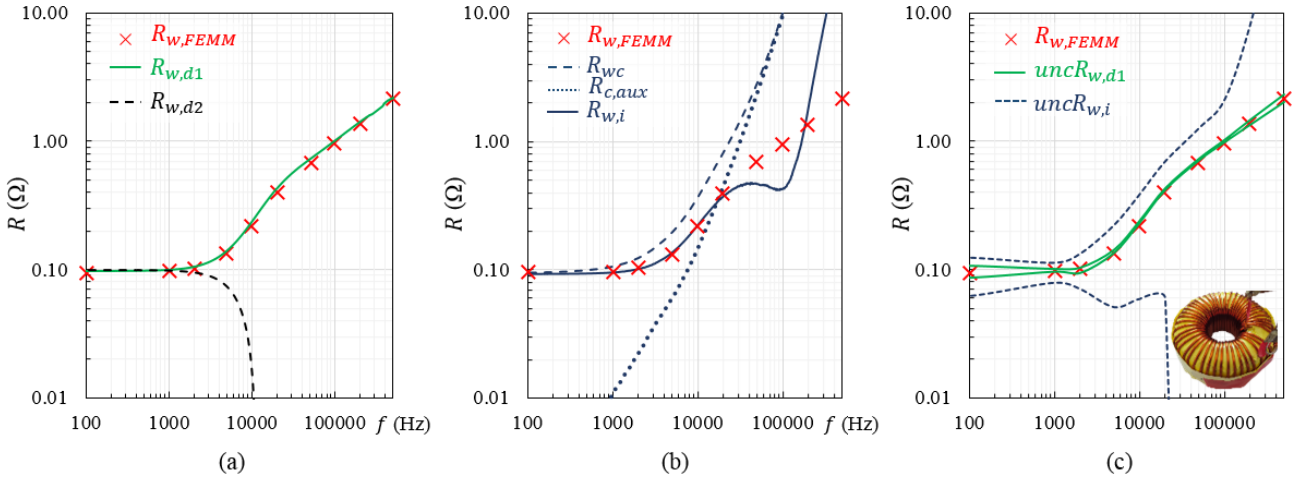

FIGURE 15. Winding resistance measured with the different techniques for the low μ toroidal inductor prototype. (a) Direct technique with the auxiliary winding in the *inside position* $R_{w,d1}$ (continuous line) and in the *outside position* $R_{w,d2}$ (dash line). (b) Indirect technique $R_{w,i}$ (continuous line), including the total inductor resistance R_{wc} (dash line) and the core resistance $R_{c,aux}$ (dot line). (c) R_w measurement uncertainty for the direct technique with the *inside position* $uncR_{w,d1}$ (continuous line) and the indirect technique $uncR_{w,i}$ (dash line). In all of them the 2D FE results $R_{w,FEMM}$ are shown (red cross).

TABLE 1. Inductor prototypes main characteristics.

Characteristics	Low μ toroidal inductor Fig.14(a)	High μ PM gapped inductor Fig.14(b)
Self-Inductance, L	2 mH @0A –1.5mH @I_p	110 µH @ 0A and I_p
Maximum current, I_p	12.5 A	7 A
Core	CH610060 (CSC HighFlux powder core with μ_{eff} = 60) [45]	PM 50/39 N27 250n (TDK ferrite 2 mm air gap) [46]
Winding	AWG13 wire, 105 turns in 2 layers	420x0.1mm P155/G1 Litz wire [47], 21 turns 3 layers
Application	dc-dc buck converter for low power electric vehicle charger	dual active bridge for automotive applications
Current waveform	9A DC fundamental, 7 App 20 kHz ripple	7 A rms @50 kHz trapezoidal
Design type	Saturation-constrained P_w=12.5 W and P_c=1.2 W, $\Delta T \approx 50$ºC	Thermally-constrained P_w=3.4 W and P_c=3.1 W, $\Delta T \approx 40$ºC

is 500 kHz for both prototypes, which is at least a decade over the fundamental current harmonic. Thus, and according to (28), in the direct technique auxiliary winding diameters ϕ_a of 0.1 mm for the toroidal inductor and of 0.05 mm for the PM gapped inductor are used ($\delta_{min} = 92$ μm at 500 kHz and 20°C). The auxiliary coupled inductors used in *step 2* of the indirect technique for the two inductors are built following the guidelines explained in Section IV.B in order to assure a zero $R_{w,m}$. It is not considered necessary here to show the effect of an incorrect design of this auxiliary coupled inductor on the R_w measurements since it has already and recently been analyzed in [20].

B. LOW μ TOROIDAL INDUCTOR

First, the direct technique with the two different locations for the auxiliary winding proposed in Fig.13 is implemented. The measured winding resistances and the calculated ones via the 2D finite element simulation are shown in Fig. 15 (a) as a function of frequency. In this figure, the measured values for the *inside position* (Fig. 12(a)) are referred to as $R_{w,d1}$ and the measured values for the *outside position* (Fig. 12(b)) are referred to as $R_{w,d2}$. It can be seen that the *inside position* of the auxiliary winding leads to a measurement in very good agreement with the simulated results. However, if the auxiliary winding is placed in the *outside position*, a big deviation between measurement and simulation is obtained for frequencies higher than 1.5 kHz. This is due to a non-zero $R_{w,m}$. The value of this resistance is non negligible for frequencies for which the diameter of the original winding ϕ (1.83 mm) is higher than the skin depth δ (1.35 kHz in this prototype). For frequencies beyond 10 kHz, $R_{w,m}$ overtakes the original winding resistance R_w and negative resistances are measured as predicted in (25). The value of $R_{w,m}$ is 0.52 Ω at 20 kHz (fundamental current harmonic) and 1.7 Ω at 100 kHz (fifth harmonic).

For the sake of clarity, it is important to understand here that measuring a negative resistance does not mean that the inductor generates energy. It is just a voltage *reflection* effect due to the points between which the voltage is measured. If the circuit in Fig. 10 is analyzed, it can be seen that the voltage drop produced by I_L in the *series* $-R_{w,m}$ is always compensated by the voltage drop produced by the same current in the *parallel* $+R_{w,m}$ and no power is generated or dissipated.

It can be concluded then that only the *inside position* proposed in this paper for the auxiliary winding (Fig. 12(a))

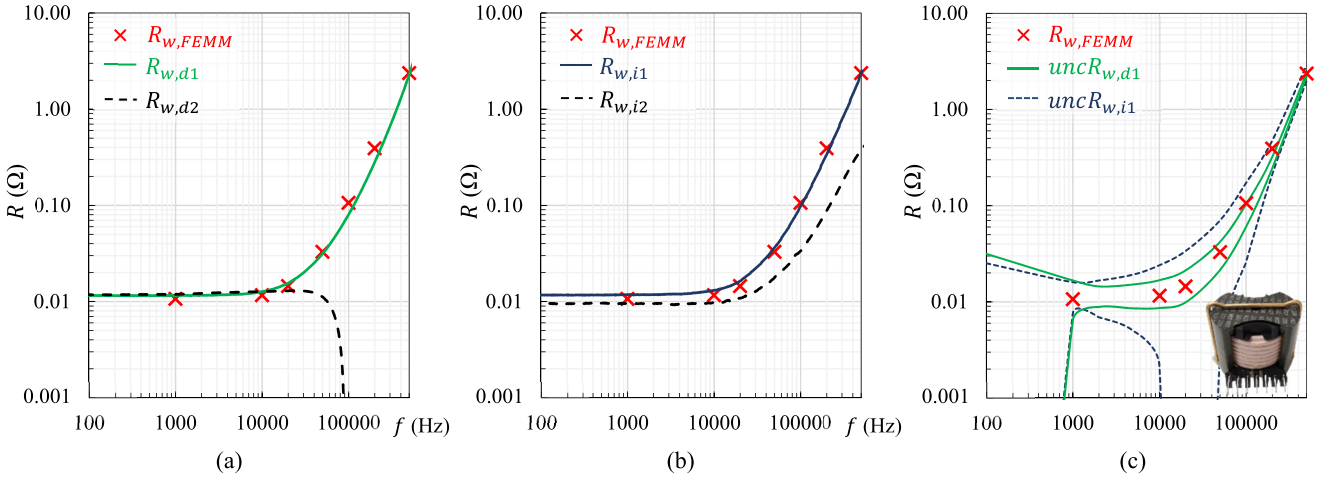

FIGURE 16. Winding resistance measured with the different techniques for the high μ gapped inductor. (a) Direct technique with the auxiliary winding in the *inside* location $R_{w,d1}$ (continuous line) and in the *outside* location $R_{w,d2}$ (dash line). (b) Indirect technique with an auxiliary coupled inductor with no gap $R_{w,i1}$ (continuous line) or with a 2 mm gap $R_{w,i2}$ (dash line). (c) R_w measurement uncertainty for the *inside* direct $uncR_{w,d1}$ (continuous line) and the *non-gapped* indirect $uncR_{w,i1}$ (dash line) techniques. In all of them the 2D FE results $R_{w,FEMM}$ are shown (red cross).

enables the direct technique to correctly measure R_w. A maximum deviation of 7.6% is obtained at 10 kHz with this technique. The obtained measurement uncertainty is also plotted in Fig. 15 (c) as the maximum and minimum boundaries ($uncR_{w,d1}$) for the true values of R_w. Measurement uncertainties of 1.2% at 20 kHz and 1.7% at 100 kHz are obtained.

Second, the indirect technique is implemented. In Fig. 15(b) the total inductor resistance measured in *step 1*, R_{wc}, the core resistance measured in *step 2*, $R_{c,aux}$, and the measured winding resistance obtained in step 3, $R_{w,i}$, are plotted. As can be seen in Fig. 15(b), important deviations in the measured $R_{w,i}$ are obtained for frequencies beyond 20 kHz. The reason for this deviations is found in the core resistance measurement in *step 2* but it is not related to the $R_{w,m}$ of the auxiliary coupled inductor. The coupled inductor has been built with 0.1 mm-diameter round wire for a zero $R_{w,m}$. The deviation is due to the fact that the same core with the same effective permeability as in the original inductor has to be used since it is not possible to remove the air gap from a core with a homogeneously distributed air gap. As the air gap cannot be removed, very high phase values are measured, even higher than 89.9° for some frequencies. This means that very high measurement uncertainty is obtained. In addition, powder cores experience *high* power loss meaning that, even with small signal excitation, the core resistance is a relevant percentage of the inductor total resistance. At frequencies over 20 kHz the core resistance becomes higher than the winding resistance to be measured. As a result, the measurement uncertainty is strongly amplified by the subtraction performed in *step 3* leading to big measurement errors for frequencies over 10 kHz and a maximum error of 55.3% at 100 kHz. The measurement uncertainty obtained with the indirect technique is plotted in Fig. 15(c) and referred to as $uncR_{w,i}$. The calculation of the measurement uncertainty for both the indirect and the direct techniques under different conditions is discussed in [21].

It can be concluded that, when applied to powder core inductors, the indirect techniques obtain unacceptable measurement uncertainties (84.5% at 20 kHz and 394% at 100 kHz) that lead to important measurement deviations. Only the direct technique with the *inside position* for the auxiliary winding proposed in this paper enables an accurate measurement of the winding resistance.

C. HIGH μ PM GAPPED INDUCTOR

First, the direct technique with the two different locations for the auxiliary winding presented in Fig.14 is implemented. The measured winding resistances and the calculated one via the 2D finite element simulation are shown in Fig. 16 (a) as a function of frequency. In this figure, the measured values for the *inside position* (Fig. 13(a)) are named $R_{w,d1}$ and the measured values for the *outside position* (Fig. 13(b)) $R_{w,d2}$. It can be seen that the *inside position* of the auxiliary winding leads to a measurement in very good agreement with the simulated results. If the auxiliary winding is placed in the *outside position*, a big deviation between measurement and simulation is obtained for frequencies higher than 20 kHz. This is again due to a non-zero $R_{w,m}$. The value of $R_{w,m}$ is 28 mΩ at 50 kHz (fundamental current) and 3.7 Ω at 500 kHz (tenth harmonic). For frequencies beyond 90 kHz, $R_{w,m}$ increases over the original winding resistance R_w and negative resistances are measured.

It can again be concluded that the location of the auxiliary winding is key for the validity of the direct technique. It has been shown here that only the *inside position* proposed in this paper enables the direct technique to correctly measure R_w. Deviations of −3.8% at 50 kHz and -3.4% at 500 kHz are obtained with this technique.

Second, the indirect technique is implemented following two different approaches. The difference lies in the way the coupled inductor is built in order to perform *step 2*. In both cases the coupled inductors are built to obtain zero $R_{w,m}$ following the guidelines presented in Section IV. In the first approach, the gap has been removed to reduce the measurement uncertainty. While in the second one, the auxiliary coupled inductor is built with the same gap as the original inductor (2 mm) in order to represent the cases in which the gap cannot be removed due to its impact on the inductor core loss as in [27], [41], and [31].

The winding resistance values measured with the indirect technique are shown in Fig. 16(b). The results with the ungapped auxiliary coupled inductor are named $R_{w,i1}$ and plotted in a continuous line and the results obtained with the 2 mm auxiliary coupled inductor, called $R_{w,i2}$, are plotted in a dash line. It can be seen that the indirect technique with the no gap approach leads to a measurement in very good agreement with the simulated results with deviations of -0.9% at 50 kHz and -2.6% at 500 kHz. However, when the gap cannot be removed important deviations in the measured $R_{w,i2}$ are obtained for frequencies beyond 20 kHz. Deviations of -45.5% at 50 kHz and -84.1% at 500 kHz are obtained which indicates that the indirect technique is not suitable for these cases.

In Fig. 16(c), the measurement uncertainties for the best versions of both R_w measurement techniques, direct $R_{w,d1}$ and indirect $R_{w,i1}$, are plotted. It can be seen that at the fundamental frequency of the current (50 kHz), the measurement uncertainty obtained with the direct technique with the *inside position* proposed in this paper is 32%, considerably lower than the 91% obtained with the best version of the indirect technique (*step 2* with no gap).

VI. CONCLUSION

The techniques for the R_w measurement in power inductors are reviewed in this paper. These techniques can be classified into two groups, indirect and direct. Both R_w measurement techniques use coupled inductors to separate winding and core power losses. If coupled inductors with non-zero winding mutual resistances $R_{w,m}$ are used, invalid results will be obtained with the R_w measurement techniques. In this paper, this fact is demonstrated and practical guidelines for the design of the zero $R_{w,m}$ coupled inductors for both techniques are given. Particularly, the location of the auxiliary winding for the direct technique is investigated. For this purpose, first coupled inductors are explained in depth with a special focus on the $R_{w,m}$ modelling and understanding.

Two inductor prototypes are built and tested, one with low μ toroidal powder core and solid round wire and the other with high μ gapped PM ferrite core and Litz wire. Their winding resistances are measured by means of both indirect and direct techniques and also calculated by means of simulation with a FEA software. It is found that, especially for low μ but also for high μ gapped inductors, the indirect technique obtain high measurement uncertainties that can lead to important deviations in the measured R_w. Only the direct technique with the *inside position* for the auxiliary winding proposed in this paper enables an accurate measurement of the winding resistance for any of the studied inductors.

ACKNOWLEDGMENT

The authors would like to thank Prof. Dr. Johann W. Kolar and the staff of the Power Electronic Systems Laboratory (PES), ETH Zürich, since it was during the first author's research stay there in 2016 when an important part of the idea behind this paper was originated.

REFERENCES

[1] M. Pavlovsky, G. Guidi, and A. Kawamura, "Assessment of coupled and independent phase designs of interleaved multiphase buck/boost DC–DC converter for EV power train," *IEEE Trans. Power Electron.*, vol. 29, no. 6, pp. 2693–2704, Jun. 2014.

[2] M. S. Perdigao, J. P. F. Trovao, J. M. Alonso, and E. S. Saraiva, "Large-signal characterization of power inductors in EV bidirectional DC–DC converters focused on core size optimization," *IEEE Trans. Ind. Electron.*, vol. 62, no. 5, pp. 3042–3051, May 2015.

[3] L. Schrittwieser, M. Leibl, M. Haider, F. Thöny, J. W. Kolar, and T. B. Soeiro, "99.3% efficient three-phase buck-type all-SiC SWISS rectifier for DC distribution systems," *IEEE Trans. Power Electron.*, vol. 34, no. 1, pp. 126–140, Jan. 2019.

[4] B. Singh, B. N. Singh, A. Chandra, K. Al-Haddad, A. Pandey, and D. P. Kothari, "A review of single-phase improved power quality AC-DC converters," *IEEE Trans. Ind. Electron.*, vol. 50, no. 5, pp. 962–981, Oct. 2003.

[5] E. Akpınar, A. Balıkcı, E. Durbaba, and B. T. Azizoğlu, "Single-phase transformerless photovoltaic inverter with suppressing resonance in improved H6," *IEEE Trans. Power Electron.*, vol. 34, no. 9, pp. 8304–8316, Sep. 2019.

[6] J. L. Agorreta, M. Borrega, J. López, and L. Marroyo, "Modeling and control of N-paralleled grid-connected inverters with LCL filter coupled due to grid impedance in PV plants," *IEEE Trans. Power Electron.*, vol. 26, no. 3, pp. 770–785, Mar. 2011.

[7] M. Zabaleta, E. Burguete, D. Madariaga, I. Zubimendi, M. Zubiaga, and I. Larrazabal, "LCL grid filter design of a multimegawatt medium-voltage converter for offshore wind turbine using SHEPWM modulation," *IEEE Trans. Power Electron.*, vol. 31, no. 3, pp. 1993–2001, Mar. 2016.

[8] G. Domingues-Olavarria, P. Fyhr, A. Reinap, M. Andersson, and M. Alaküla, "From chip to converter: A complete cost model for power electronics converters," *IEEE Trans. Power Electron.*, vol. 32, no. 11, pp. 8681–8692, Nov. 2017.

[9] L. Schrittwieser, J. W. Kolar, and T. B. Soeiro, "99% efficient three-phase buck-type SiC MOSFET PFC rectifier minimizing life cycle cost in DC data centers," *CPSS Trans. Power Electron. Appl.*, vol. 2, no. 1, pp. 47–58, Apr. 2017.

[10] Z. Zhang, K. D. T. Ngo, and J. L. Nilles, "Design of inductors with significant AC flux," *IEEE Trans. Power Electron.*, vol. 32, no. 1, pp. 529–539, Jan. 2017.

[11] W. G. Hurley and W. H. Wölfle, "Inductor design," in *Transformers Inductors for Power Electronics: Theory, Design and Applications*, 1st ed. Chischester, U.K.: Wiley, 2013, ch. 3.

[12] E. L. Barrios, A. Urtasun, A. Ursúa, L. Marroyo, and P. Sanchis, "Optimal DC gapped inductor design including high-frequency effects," in *Proc. 41st Annu. Conf. IEEE Ind. Electron. Soc. (IECON)*, Nov. 2015, pp. 003928–003933.

[13] D. Elizondo, E. L. Barrios, P. Sanchis, and A. Ursua, "Analytical modeling of high-frequency winding loss in round-wire toroidal inductors," in *Proc. IEEE 21st Workshop Control Modeling Power Electron. (COMPEL)*, Nov. 2020, pp. 1–6.

[14] C. R. Sullivan, "Computationally efficient winding loss calculation with multiple windings, arbitrary waveforms, and two-dimensional or three-dimensional field geometry," *IEEE Trans. Power Electron.*, vol. 16, no. 1, pp. 142–150, Jan. 2001.

[15] W. A. Roshen, "Fringing field formulas and winding loss due to an air gap," *IEEE Trans. Magn.*, vol. 43, no. 8, pp. 3387–3394, Aug. 2007.

[16] E. L. Barrios, A. Ursua, L. Marroyo, and P. Sanchis, "Analytical winding loss calculation for high-frequency low-permeability inductors," in *Proc. IEEE 18th Workshop Control Modeling Power Electron. (COMPEL)*, Stanford, CA, USA, Jul. 2017, pp. 1–7.

[17] T. Ge, B. Carpenter, and K. D. T. Ngo, "Design methodology of a one-turn inductor with significant DC and AC fluxes—Demonstration in a resonant cross-commutated Buck converter," *IEEE Trans. Ind. Electron.*, vol. 66, no. 11, pp. 8424–8433, Nov. 2019.

[18] W. Wang, F. Pansier, S. de Haan, and J. A. Ferreira, "Novel and simple calorimetric methods for quantifying losses in magnetic core and GaN transistor in a high frequency boost converter," *Chin. J. Elect. Eng.*, vol. 2, no. 2, pp. 68–75, Dec. 2016.

[19] B. X. Foo, A. L. F. Stein, and C. R. Sullivan, "A step-by-step guide to extracting winding resistance from an impedance measurement," in *Proc. IEEE Appl. Power Electron. Conf. Expo. (APEC)*, Tampa, FL, USA, Mar. 2017, pp. 861–867.

[20] K. Niyomsatian, J. J. C. Gyselinck, and R. V. Sabariego, "Experimental extraction of winding resistance in litz-wire transformers—Influence of winding mutual resistance," *IEEE Trans. Power Electron.*, vol. 34, no. 7, pp. 6736–6746, Jul. 2019.

[21] F. N. Javidi and M. Nymand, "A new method for measuring winding AC resistance of high-efficiency power inductors," *IEEE Trans. Power Electron.*, vol. 33, no. 12, pp. 10736–10747, Dec. 2018.

[22] C. Feeney, J. Zhang, and M. Duffy, "AC winding loss of phase-shifted coupled windings," *IEEE Trans. Power Electron.*, vol. 31, no. 2, pp. 1472–1478, Feb. 2016.

[23] J. H. Spreen, "Electrical terminal representation of conductor loss in transformers," *IEEE Trans. Power Electron.*, vol. 5, no. 4, pp. 424–429, Oct. 1990.

[24] M. S. Rylko, B. J. Lyons, J. G. Hayes, and M. G. Egan, "Revised magnetics performance factors and experimental comparison of high-flux materials for high-current DC–DC inductors," *IEEE Trans. Power Electron.*, vol. 26, no. 8, pp. 2112–2126, Aug. 2011.

[25] R. A. Torres, H. Dai, T. M. Jahns, and B. Sarlioglu, "Design of high-performance toroidal DC-link inductor for current-source inverters," in *Proc. IEEE Appl. Power Electron. Conf. Expo. (APEC)*, Anaheim, CA, USA, Mar. 2019, pp. 2694–2701.

[26] J. Imaoka, K. Okamoto, M. Shoyama, Y. Ishikura, M. Noah, and M. Yamamoto, "Modeling, magnetic design, simulation methods, and experimental evaluation of various powder cores used in power converters considering their DC superimposition characteristics," *IEEE Trans. Power Electron.*, vol. 34, no. 9, pp. 9033–9051, Sep. 2019.

[27] G. Calderon-Lopez, Y. Wang, and A. J. Forsyth, "Mitigation of gap losses in nanocrystalline tape-wound cores," *IEEE Trans. Power Electron.*, vol. 34, no. 5, pp. 4656–4664, May 2019.

[28] J. A. Ferreira, "Improved analytical modeling of conductive losses in magnetic components," *IEEE Trans. Power Electron.*, vol. 9, no. 1, pp. 127–131, Jan. 1994.

[29] C. P. Steinmetz, "On the law of hysteresis," *Proc. IEEE*, vol. 72, no. 2, pp. 197–221, Feb. 1984.

[30] Y. Han, G. Cheung, A. Li, C. R. Sullivan, and D. J. Perreault, "Evaluation of magnetic materials for very high frequency power applications," *IEEE Trans. Power Electron.*, vol. 27, no. 1, pp. 425–435, Jan. 2012.

[31] D. Neumayr, D. Bortis, J. W. Kolar, S. Hoffmann, and E. Hoene, "Origin and quantification of increased core loss in MnZn ferrite plates of a multi-gap inductor," *CPSS Trans. Power Electron. Appl.*, vol. 4, no. 1, pp. 72–93, Mar. 2019.

[32] J. Muhlethaler, J. Biela, J. W. Kolar, and A. Ecklebe, "Core losses under the DC bias condition based on Steinmetz parameters," *IEEE Trans. Power Electron.*, vol. 27, no. 2, pp. 953–963, Feb. 2012.

[33] H. Y. Lu, J. Guo Zhu, and S. Y. R. Hui, "Experimental determination of stray capacitances in high frequency transformers," *IEEE Trans. Power Electron.*, vol. 18, no. 5, pp. 1105–1112, Sep. 2003.

[34] L. Dalessandro, F. da Silveira Cavalcante, and J. W. Kolar, "Self-capacitance of high-voltage transformers," *IEEE Trans. Power Electron.*, vol. 22, no. 5, pp. 2081–2092, Sep. 2007.

[35] T. Guillod, F. Krismer, and J. W. Kolar, "Magnetic equivalent circuit of MF transformers: Modeling and parameter uncertainties," *Electr. Eng.*, vol. 100, no. 4, pp. 2261–2275, May 2018.

[36] C. Carretero, "Coupling power losses in inductive power transfer systems with litz-wire coils," *IEEE Trans. Ind. Electron.*, vol. 64, no. 6, pp. 4474–4482, Jun. 2017.

[37] H. H. Cui, M. H. Kao, L. L. Xue, and K. D. T. Ngo, "Enhanced inductance and winding loss model for coupled inductors," in *Proc. IEEE Energy Convers. Congr. Expo. (ECCE)*, Oct. 2020, pp. 3518–3523.

[38] W. G. Hurley, E. Gath, and J. G. Breslin, "Optimizing the AC resistance of multilayer transformer windings with arbitrary current waveforms," *IEEE Trans. Power Electron.*, vol. 15, no. 2, pp. 369–376, Mar. 2000.

[39] F. D. Tan, J. L. Vollin, and S. M. Cuk, "A practical approach for magnetic core-loss characterization," *IEEE Trans. Power Electron.*, vol. 10, no. 2, pp. 124–130, Mar. 1995.

[40] V. J. Thottuvelil, T. G. Wilson, and H. A. Owen, "High-frequency measurement techniques for magnetic cores," *IEEE Trans. Power Electron.*, vol. 5, no. 1, pp. 41–53, Jan. 1990.

[41] B. Cougo, A. Tuysüz, J. Muhlethaler, and J. W. Kolar, "Increase of tape wound core losses due to interlamination short circuits and orthogonal flux components," in *Proc. 37th Annu. Conf. IEEE Ind. Electron. Soc. (IECON)*, Melbourne, VIC, Australia, Nov. 2011, pp. 1372–1377.

[42] M. Mu, Q. Li, D. J. Gilham, F. C. Lee, and K. D. T. Ngo, "New core loss measurement method for high-frequency magnetic materials," *IEEE Trans. Power Electron.*, vol. 29, no. 8, pp. 4374–4381, Aug. 2014.

[43] D. Meeker. (2004). *Finite Element Magnetic Method Software*. [Online]. Available: http://www.femm.info/wiki/HomePage

[44] Keysight Technologies. *E4990A Impedance Analyzer, 20 Hz to 120 MHz*. Accessed: May 2021. [Online]. Available: https://www.keysight.com/en/pd-2405177-pn-E4990A

[45] Chang Sung Corporation. *Magnetic Powder Core Catalog*. Accessed: May 2021. [Online]. Available: https://mrccomponents.com/downloads/csc/general/2018-09-04-00-CSC_PowderCores_e-calague_2018-08-29.pdf

[46] EPCOS AG. (May 2017). *Ferrite and Accessories, PM 50/39, Core and Accessories*. [Online]. Available: https://www.tdk-electronics.tdk.com/inf/80/db/fer/pm_50_39.pdf

[47] ELEKTRISOLA. *HF Litz Wire, Technical Data by Dimensions*. Accessed: May 2021. [Online]. Available: https://www.elektrisola.com/en/Products/Litz-Wire/Dimensions

ERNESTO L. BARRIOS (Member, IEEE) was born in Pamplona, Spain, in 1988. He received the B.Sc., M.Sc., and Ph.D. degrees in electrical engineering from the Public University of Navarre, Pamplona, in 2009, 2012, and 2015, respectively. In 2011, he joined the Electrical Engineering, Power Electronics and Renewable Energy Research Group, Public University of Navarre, where he is currently an Associate Professor and a Researcher. For six months in 2016, he was an Academic Guest with the Power Electronic Systems Laboratory, ETH Zürich, Zürich, Switzerland. His research interests include high-frequency magnetics, power electronics, and renewable energies.

DAVID ELIZONDO (Student Member, IEEE) was born in Pamplona, Spain. He received the B.Sc. degree (Hons.) in electrical engineering and the M.Sc. degree (Hons.) in renewable energies and electrical engineering from the Public University of Navarre (UPNA), in 2017 and 2019, respectively, where he is currently pursuing the Ph.D. degree with a focus on the design of power converters for EV charging. He developed his master's thesis at Hochschule Osnabrück, Germany. In 2017, he joined the Electrical Engineering, Power Electronics and Renewable Energy Research Group, UPNA. His research interests include EV fast-charging stations, resonant converters, and power inductors.

ALFREDO URSÚA (Senior Member, IEEE) received the B.Sc. and M.Sc. degrees (Hons.) in electrical engineering and the Ph.D. degree in industrial engineering from the Public University of Navarre (UPNA), Spain, in 2001, 2004, and 2010, respectively.

In 2002, he joined the Department of Electrical, Electronic and Communications Engineering, where he is currently an Associate Professor. He is also working with the Electrical Engineering, Power Electronics and Renewable Energy Research Group, UPNA Institute of Smart Cities (ISC). He is currently the Vice Dean of the School of Industrial and ICT Engineering and a member of the Steering Committee of the University Chair for Renewable Energies. He has been involved in more than 60 research projects both with public funding and in cooperation with industry. He is the co-inventor of two patents. He has supervised three Ph.D. thesis and coauthored more than 70 articles and contributions in international journals, conferences, and three book chapters. His research interests include renewable energy systems, electric energy storage technologies, power electronics, energy management, and electric microgrids.

Dr. Ursúa received the UPNA Research Award for the Best Technical Paper, in 2013, and the Extraordinary Doctoral Award in the field of telecommunication technologies, bioengineering, and renewable energies.

PABLO SANCHIS (Senior Member, IEEE) received the M.Sc. degree in electrical engineering, the M.Sc. degree in management and business administration, and the Ph.D. degree in electrical engineering from the Public University of Navarre (UPNA), Pamplona, Spain, in 1994, 1995, and 2002, respectively.

From 1996 to 1998, he was a Guest Researcher with the Delft University of Technology, Delft, The Netherlands. In 1998, he joined the Department of Electrical, Electronic and Communications Engineering, UPNA, where he is currently a Professor. He was the Vice Dean of the School of Industrial and ICT Engineering and the Director of the University Unit for Research Resources and Structures. He is currently the Director of the UPNA Chair for Renewable Energies and the Head of the Electrical Engineering, Power Electronics, and Renewable Energies Research Group. He has been involved in more than 100 research projects both with public funding and in cooperation with industry. He is the co-inventor of ten patents. He has supervised ten Ph.D. theses and coauthored more than 140 articles and contributions in international journals, conferences, and five book chapters (H-index of 32). His current research interests include renewable energies, power electronics, electric energy storage technologies, grid integration of renewable energies, and electric microgrids.

Dr. Sanchis received the UPNA Research Award for the Best Technical Paper, in 2013, and the UPNA Excellence in Teaching Award, in 2017.